Research in Astronomy and Astrophysics, 22:125018 (13pp), 2022 December https://doi.org/10.1088/1674-4527/ac9e92

Machine Learning to Search for Accreting Neutron Star Binary Candidates Using Chinese Space Station Telescope Photometric System

Shun-Yi Lan[1,2,3], Kai-Fan Ji[1], and Xiang-Cun Meng[1,2]
[1] Yunnan Observatories, Chinese Academy of Sciences, Kunming 650216, China; lanshunyi@ynao.ac.cn, xiangcunmeng@ynao.ac.cn
[2] Key Laboratory for the Structure and Evolution of Celestial Objects, Chinese Academy of Sciences, Kunming 650216, China
[3] University of Chinese Academy of Sciences, Beijing 100049, China
Received 2022 September 19; revised 2022 October 17; accepted 2022 October 21; published 2022 December 7

Abstract

Accreting neutron star binary (ANSB) systems can provide some important information about neutron stars (NSs), especially on the structure and the equation of state of NSs. However, only a few ANSBs are known so far. The upcoming Chinese Space Station Telescope (CSST) provides an opportunity to search for a large number of ANSB candidates. We aim to investigate whether or not a machine learning method may efficiently search for ANSBs based on CSST photometric system. In this paper, we generate some ANSBs and normal binaries under CSST photometric system by binary evolution and binary population synthesis method and use a machine learning method to train a classification model. We consider the classical multi-color disk and the irradiated accretion disk, then compare their effects on the classification results. We find that no matter whether the X-ray reprocessing effect is included or not, the machine learning classification accuracy is always very high, i.e., higher than 96%. If a significant magnitude difference exists between the accretion disk and the companion of an ANSB, machine learning may not distinguish it from some normal stars such as massive main sequence stars, white dwarf binaries, etc. False classifications of the ANSBs and the normal stars highly overlap in a color–color diagram. Our results indicate that machine learning would be a powerful way to search for potential ANSB candidates from the CSST survey.

Key words: stars: neutron – X-rays: binaries – methods: analytical

1. Introduction

According to the recycling scenario, a millisecond pulsar (MSP) is an old neutron star (NS) that has been spun up to a high rotation frequency by mass accretion from its companion in a binary system (see Bhattacharya & van den Heuvel 1991 for a review). During the accretion phase, the accreting neutron star binary (ANSB) manifests itself as an X-ray source. When mass transfer ceases, the binary hosts a radio MSP. The discovery of accreting millisecond X-ray pulsar (AMXP) SAX J1808.4-3658 (Wijnands & van der Klis 1998) and transitional MSPs (Archibald et al. 2009; Papitto et al. 2013; Bassa et al. 2014) strongly support the recycling scenario. The ANSBs may also provide information about the structure of NSs and constrain the binary evolution (e.g., Patterson 1984; Baillot d'Etivaux et al. 2019).

Depending on the mass of the companion star, most ANSBs can be divided into two categories: low-mass X-ray binary (LMXB) and high-mass X-ray binary (HMXB), the remaining small part is intermediate-mass X-ray binary (IMXB). HMXBs generally leave behind double NSs and partially recycle the first-born NS, and HMXBs will not be discussed in this paper. Moreover, some ANSBs are persistent X-ray sources, while others are transient sources. Accretion driven transient sources are thought to be derived from the instability of the accretion disk, where the mass transfer rate between the NS and its companion is lower than a critical mass transfer rate (Lasota 2001). In this paper, the ANSBs we produce are either persistent sources or transient sources in the quiescent state.

The origin of the NUV/optical emission of ANSBs is quite complex and several mechanisms may contribute to the NUV/optical emission together. First, the accretion disk due to viscous heating and irradiation by X-ray may partly contribute to the NUV/optical emission. In particular, Russell et al. (2006) found that there is a correlation between X-ray and NUV/optical emission in the hard state of LMXB, which indicates that at least in the hard state, the optical emission from the irradiation by X-ray, i.e., the X-ray reprocessing effect, maybe the dominant mechanism. Second, companion stars may partly contribute to the NUV/optical emission. Finally, the NUV/optical emission may also be produced in jet or in hot flow (e.g., Homan et al. 2005). Here, we will mainly investigate the contribution of accretion disk and companion, and will consider other mechanisms step by step to complete our model in the future.

ANSB plays an important role in the theory of binary evolution and the formation of MSPs. However, only a few

Table 1
Designed Parameters of CSST Photometric Surveys

Bands	NUV	*u*	*g*	*r*	*i*	*z*	*y*
Wavelength (nm)	255–317	322–396	403–545	554–684	695–833	846–1000	937–1000
Exposure time (s)	150*4	150*2	150*2	150*2	150*2	150*2	150*4
Sensitivity (AB mag)	25.4	25.4	26.3	26.0	25.9	25.2	24.4

Note. The CSST NUV*ugrizy* magnitudes are given in AB system, and the sensitivities are given under 5σ limits.

ANSBs have been observed so far (e.g., Ritter & Kolb 2003; Liu et al. 2007). The classification of ANSBs is normally based on the spectra obtained from optical identification and mass function from X-ray timing, on the X-ray timing properties, such as the coherent pulsations (Patruno & Watts 2021), and on the presence of thermonuclear burst (see Cumming 2004 for a review). In addition to these methods, identification can also be done by comparison with known sources.

Although the recycling scenario is widely accepted, there are still some open problems. Why do not most LMXBs have pulsation (e.g., Vaughan et al. 1994; Patruno et al. 2018)? What is the relation between AMXPs and black widow/redback pulsars (e.g., di Salvo et al. 2008; Hartman et al. 2008)? What is the mechanism of optical or UV pulsation (e.g., Ambrosino et al. 2021; Jaodand et al. 2021)? We do not continue to list other open problems here, but it should be pointed out that these problems are mainly caused by the fact that there is not a complete sample of LMXB[4] or AMXP (Patruno & Watts 2021). Then, building a complete sample becomes necessary to solve these problems. The upcoming Chinese Space Station Telescope (CSST) could provide an opportunity to build such a sample. CSST is a 2 m space telescope and is planned to launch in 2024. CSST will be in the same orbit as the China Manned Space Station. The survey from CSST will have seven photometric imaging bands covering 255–1000 nm, with large field of view $\sim 1\ \mathrm{deg}^2$, and a high-spatial resolution $\sim 0\farcs15$ (see Table 1) (Cao et al. 2018; Gong et al. 2019). In this work, we try to investigate whether or not machine learning can efficiently search for ANSB candidates from CSST photometric data, based on the systems from the accretion-induced-collapse (AIC) channel.

In Section 2 we describe our methods. We show the machine learning classification results in Section 3. Discussions and conclusions are given in Sections 4 and 5, respectively.

2. Method

A massive ONeMg WD in a close binary can produce an NS via AIC channel. The companion of the ONeMg WD can be an MS, a red giant (RG), or a He star. The NS can spin up by accreting material from its companion. The MSPs produced from this channel are very similar to those from a standard channel. However, the AIC channel can help to explain the young pulsars found in the globular clusters (Tauris et al. 2013; Wang 2018). All the ANSBs that we generate in this paper are produced by the AIC channel. The evolutionary details of pre- and post-AIC are similar to Meng & Podsiadlowski (2017) and Wang et al. (2022), and we do not show too many repetitive details here.

We assume that the NS in an ANSB system is a point mass. The radiation of an ANSB comes mainly from the accretion disk and the companion. As mentioned in Section 1, the composition of radiation of ANSB is complex, especially at the optical wavelength. Although some models have been proposed, uncertainties still exist. Here, we use two different accretion disk models step by step to check the effect of the different radiation mechanisms on machine learning classification efficiency.

2.1. Classical Multi-color Disk

We first use the classical multi-color disk (MCD) model to calculate the radiation flux from the accretion disk by the following equation (Mitsuda et al. 1984):

$$f_{\mathrm{d}}(E) = \frac{\cos\theta}{D^2}\int_{r_{\mathrm{in}}}^{r_{\mathrm{out}}} 2\pi r B(E, T) dr = \frac{8\pi r_{\mathrm{in}}^2 \cos\theta}{3D^2}\int_{T_{\mathrm{out}}}^{T_{\mathrm{in}}} \left(\frac{T}{T_{\mathrm{in}}}\right)^{-\frac{11}{8}} B(E, T)\frac{dT}{T_{\mathrm{in}}}, \tag{1}$$

where the orbital inclination angle is set to be $\theta = 60^\circ$, the inner and the outer boundary of the MCD are r_{in} and r_{out} respectively, $B(E,\ T)$ is the Planckian distribution, and $T_{\mathrm{in}} = T(r_{\mathrm{in}})$ and $T_{\mathrm{out}} = T(r_{\mathrm{out}})$. Here, r_{in} is given by Ghosh & Lamb (1979):

$$r_{\mathrm{in}} = 22\ \mathrm{km}\left(\frac{\dot{M}}{0.1\dot{M}_{\mathrm{Edd}}}\right)^{-2/7}\left(\frac{M}{1.4}\right)^{-5/7}, \tag{2}$$

and r_{out} is set to be slightly smaller than the Roche lobe radius of the NS, which cannot significantly affect our results. The temperature at radius r is calculated by the following equation

[4] Two catalogs for LMXBs: https://heasarc.gsfc.nasa.gov/W3Browse/all/lmxbcat.html, https://heasarc.gsfc.nasa.gov/W3Browse/all/ritterlmxb.html.

(Kubota et al. 1998):

$$T_{\rm eff}(r) = \left[\frac{3GM_X\dot{M}}{8\pi\sigma r^3}\left(1-\beta\sqrt{\frac{r_{\rm in}}{r}}\right)\right]^{\frac{1}{4}}, \tag{3}$$

where M_X is the mass of the compact object, $\dot{M}$ is the mass transfer rate, G is the gravity constant, σ is the Stefan–Boltzmann constant, and β is a constant depending on the disk model. Under the MCD model we choose, $\beta = 0$. The above equations imply that the ANSBs we produce are either persistent sources or transient sources in the quiescent state. We calculate the absolute magnitudes of the accretion disk under the CSST photometric system (Cao et al. 2018; Gong et al. 2019) by using the following equation:

$$m_{{\rm d},k} = -2.5\log\left[\frac{\int f_{\lambda,10{\rm pc}}S_{\lambda,k}d\lambda}{\int f_\lambda^0 S_{\lambda,k}d\lambda}\right], \tag{4}$$

where $f_{\lambda,10{\rm pc}}$ is the absolute flux of the accretion disk, $f_\nu^0 = \lambda^2 c^{-1} f_\lambda^0 = 10^{\frac{48.60}{-2.5}}\ {\rm erg\ s^{-1}\ cm^{-2}\ Hz^{-1}}$ is the flux of reference spectrum. $m_{{\rm d},k}$ is the calculated absolute magnitude of the accretion disk for the $k^{\rm th}$ band, and $S_{\lambda,k}$ is the transmission of the CSST's $k^{\rm th}$ photometric filter (Cao et al. 2018; Gong et al. 2019).

We also test the effect of other orbital inclination angles and calculate the magnitudes of the disk for other orbital inclination angles by the following equation:

$$m_{{\rm d},k}^{\alpha} - m_{{\rm d},k}^{60\circ} = -2.5\log\frac{f_{{\rm d},\alpha}}{f_{{\rm d},60\circ}}, \tag{5}$$

where $m_{{\rm d},k}^{\alpha}$ and $f_{{\rm d},\alpha}$ are the magnitude and the flux of the accretion disk for the other orbital inclination angles respectively. Here, for simplicity, we test three other inclination angles, i.e., $\alpha = 0°$, $30°$ and $85°$.

We calculate the magnitudes of the companion star from the blackbody spectrum based on the radius and the temperature of the companion star. The total magnitude of an unresolved binary system is given by the following equation (Xin et al. 2015):

$$m_i = m_{1,i} - 2.5\times\log(1+10^{\frac{m_{1,i}-m_{2,i}}{2.5}}), \tag{6}$$

where m_i, $m_{1,i}$ and $m_{2,i}$ are the $i^{\rm th}$ band magnitudes of the binary, the primary and the secondary, respectively.

The background normal stars are generated by a binary population synthesis (BPS) method (Hurley et al. 2000, 2002), in which all the systems are evolving in binaries (see Meng et al. 2009 and Meng & Podsiadlowski (2017) for details). We generate different age background normal binaries, range from 1 Myr to 14 Gyr, and use the YBC database[5] to get their CSST magnitudes directly (Chen et al. 2019). We assume that if the orbital period of a binary system is shorter than 100 yr, the system is a physical binary and we use Equation (6) to calculate its synthetic magnitude. For a system with an orbital period of larger than 100 yr, we assume it as two distinguishable objects. Here, we produce 238,340 ANSBs and 3,141,595 normal background stars.

We assume that the total photometry magnitude from systematic error of CSST fulfill the Gaussian distribution and set $\sigma = 0.05$, 0.03, 0.020, 0.02, 0.02, 0.05, 0.05 for NUV, u, g, r, i, z, y bands, respectively.

There must be extinction for observations and we apply the interstellar dust extinction law from Wang & Chen (2019):

$$\frac{A_\lambda}{A_{\rm V}} = 1.0 + 0.7499Y - 0.1086Y^2 - 0.08909Y^3 + 0.02905Y^4 + 0.01069Y^5 + 0.001707Y^6 - 0.001002Y^7, \tag{7}$$

where $Y = 1/\lambda(\mu{\rm m}) - 1.82$. Here, for simplicity, we set $A_{\rm V} = 0.5$.

Since CSST may not provide the distance information directly, we use the following equation to eliminate the constraint from the distance:

$$m'_k = m_k - \frac{\sum_{j=1}^{7} m_j}{7}, \tag{8}$$

which actually turns the seven magnitudes into some kinds of colors.

After all the above procedures, we label these magnitudes m'_k and randomly split them into two sets: a training set and a test set. After training, use the test set to evaluate the performance of the classification model. We use a multi-layer-perceptron (MLP) for classification training (Pedregosa et al. 2011). The MLP is a supervised learning algorithm, which can learn a nonlinear function approximator for either classification or regression. The MLP can also use partial fit to update the classification model in the future by real observation data of CSST.

2.2. Irradiated Accretion Disk

Due to disk instability, there are two types of ANSBs: transient sources and persistent sources. There is evidence that the optical emission of persistent sources and transient sources in bursts are strongly affected by the X-ray reprocessing effect (van Paradijs & McClintock 1994; Russell et al. 2006). In this step, we use the irradiated accretion disk (IAD) model that takes the X-ray reprocessing effect into account and train a new machine learning classification model.

The irradiation temperature at a radius of the accretion disk r is given by de Jong et al. (1996)

$$T_{\rm irr} = \left[\frac{L_{\rm X}}{4\pi\sigma r^2}\frac{H}{r}(1-\gamma)(\xi-1)\right]^{1/4}, \tag{9}$$

where $L_{\rm X}$ is the accretion luminosity and is constrained by Eddington luminosity, H is the scale height of the accretion

[5] http://stev.oapd.inaf.it/YBC/

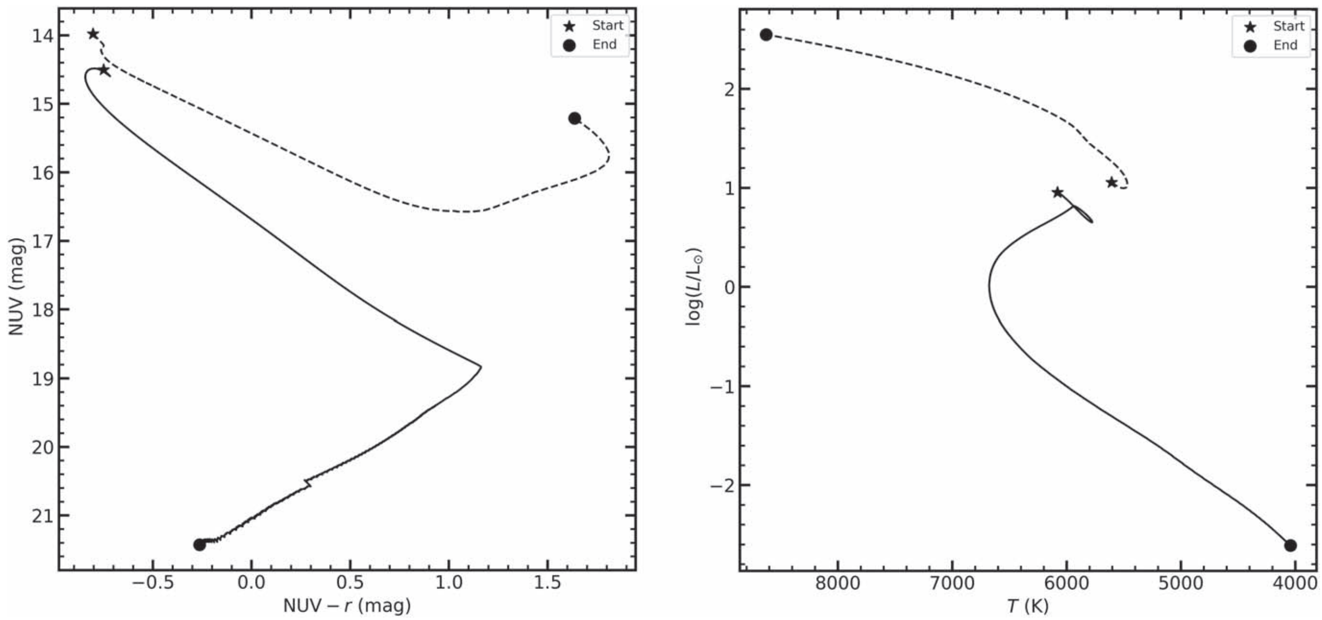

Figure 1. Two examples of ANSB systems. The left panel shows the evolutional track of the mass transfer phase of the system in CMD. The right panel shows the corresponding companion's evolutional track in HRD. The initial parameters are [$M_2^{\rm i}$, $\log(P_{\rm orb}\ {\rm day}^{-1})$] = (3.0 $M_\odot$, 0.2) and [$M_2^{\rm i}$, $\log(P_{\rm orb}\ {\rm day}^{-1})$] = (3.0 $M_\odot$, 0.5) for solid and dashed lines, respectively. $M_2^{\rm i}$ is the initial mass of the companion, and $P_{\rm orb}$ is the initial orbital period. The stars and dots represent the beginning and end of evolution, respectively. The orbital inclination angles for both systems are set to be 60°, and the distances are 10 kpc.

disk, γ is the X-ray albedo of the accretion disk, and $\xi \equiv d\ln H/d\ln r$. For simplicity, we adopt values of $\xi = 9/7$, $\gamma = 0.9$, and $H/r = 0.2$ (Vrtilek et al. 1990; de Jong et al. 1996). Following Coriat et al. (2012), we define the effective temperature of the accretion disk at a given radius:

$$T_{\rm eff}^4(r) = T_{\rm vis}^4(r) + T_{\rm irr}^4(r), \tag{10}$$

where $T_{\rm vis}(r)$ is the viscosity temperature of the accretion disk.

Similar to Section 2.1, we can calculate the absolute magnitudes of an ANSB under the CSST photometric system. We also use MLP for classification training.

3. Results

To conveniently analyze our results, we define the following criterion to assess the relation of magnitude between the accretion disk and the companion:

$$S = \sum_{k=1}^{7}(m_{{\rm d},k} - m_{{\rm c},k}), \tag{11}$$

where $m_{{\rm d},k}$ is the magnitude of the accretion disk of $k^{\rm th}$ band, and $m_{{\rm c},k}$ is the magnitude of the companion of $k^{\rm th}$ band. $S < 0$ indicates that the accretion disk is brighter than the companion, and $S > 0$ indicates that the accretion disk is dimmer than the companion. This is not a very rigorous criterion, but enough for us to analyze our results.

3.1. MCD Only

In Figure 1, we show the evolutionary tracks of two typical ANSBs with orbital periods longer (dashed line) and shorter (solid line) than the bifurcation period in color–magnitude diagram (CMD) and the evolutionary tracks of the companions in Hertzsprung–Russell diagram (HRD), respectively. The evolutionary tracks are quite different because of their different initial orbital period. For the solid lines in Figure 1, the initial orbital period of the system is shorter than the bifurcation period. The companion star evolves along the main sequence until it turns into a brown dwarf with a mass of 0.025 $M_\odot$, where our code breaks down. For the dashed lines in Figure 1, the initial orbital period of the system is longer than the bifurcation period. The companion star evolves to RG, during which the companion star maintains a high luminosity until mass transfer stops. For details of binary evolution and the evolution of ultra-compact binary, please refer to, e.g., Tutukov et al. (1985), Podsiadlowski et al. (2002), van der Sluys et al. (2005a), and van der Sluys et al. (2005b). We do not discuss too many details here.

Figures 2 and 3 show the spectral energy distribution (SED) of the beginning and end of mass transfer for two typical systems, which are the same as shown in Figure 1. In the left panel of Figure 2, the accretion disk is dimmer than, but comparable with the companion star due to the large mass of the companion star. In the right panel of Figure 2, the companion star is as low as 0.025 $M_\odot$ where our code is broken

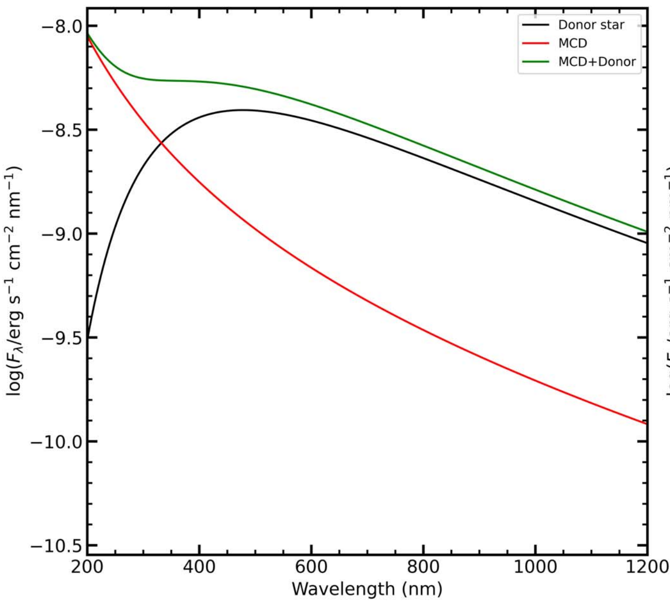

Figure 2. The SED of an ANSB at the beginning (left) and the end (right) of the mass transfer, respectively. The initial parameters are $[M^{\rm i}, \log(P_{\rm orb}\ {\rm day}^{-1})] = (3.0\,M_\odot, 0.2)$. The red lines are deduced from the MCD model, and the black lines are deduced from blackbody spectra based on the temperature and radius of the companion. The green lines represent the total flux from the system. The distance is set to 10 pc.

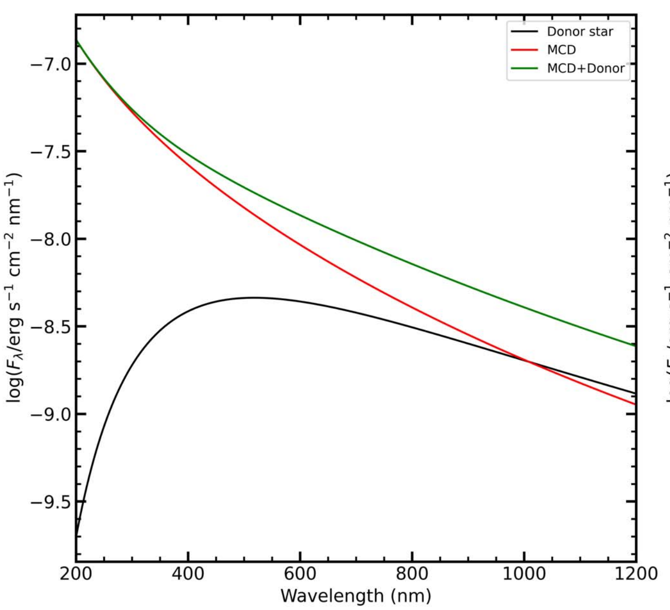

Figure 3. Similar to Figure 2, but for the system with initial parameters $[M^{\rm i}, \log(P_{\rm orb}\ {\rm day}^{-1})] = (3.0\,M_\odot, 0.5)$.

down. The flux of the companion is much lower than that of the accretion disk. In the left panel of Figure 3, the system has a high accretion rate at the beginning of the mass transfer phase, and the flux of the accretion disk is relatively large, i.e., the flux from the accretion disk is larger than, but still comparable with that from the companion. In the right panel of Figure 3, the companion is a post RG star, which is much brighter than the accretion disk at the phase of ending mass transfer. The two figures indicate that our model covers a rather large part of evolutional stages for an ANSB.

Table 2 shows the classification results of the test set. Classification accuracy of ANSBs is 97.05% and can exceed

Table 2
Classification Results of the Test Set

	All	Falsely Classified	Correctly Classified
ANSBs	116,672	1332	115,340
Normal Stars	1,454,126	3504	1,450,622
All	1,570,798	4836	1,565,962

99% for normal stars, which indicates that the machine learning method is very efficient to search for ANSBs under the CSST photometric systems. It should be noted that the numbers shown in Table 2 are not the potential observable numbers of CSST.

The types of falsely classified ANSB systems are important for analyzing the performance of the classification model. Figure 4 shows the falsely classified ANSBs in the CMD from two different perspectives. In the left panel of Figure 4, the colored dots represent the falsely classified ANSB systems in which the accretion disks are brighter or dimmer than the companion stars. These two types of systems are distributed in bluer and redder regions in the CMD, respectively. The right panel of Figure 4 shows the falsely classified ANSB systems for different orbital inclination angles. All the systems with an orbital inclination of 85° are those whose accretion disks are dimmer than their companions. Due to the low mass transfer rate of the system and the high temperature and luminosity of the companion star, the accretion disks of some falsely classified ANSB systems with other inclination angles are dimmer than the companion stars, as shown in Figure 5. In the falsely classified ANSB systems, the types of companion stars can be used to analyze the relationship between the accretion disk and the companion star. Figure 5 shows the companions in HRD for the falsely classified ANSB systems. Most of these companions are bright hot giant stars.

There are generally significant magnitude differences between the accretion disk and the companion for the falsely classified ANSB systems. Different evolution stages of the companion may contribute to the false classification, e.g., when the companions are bright hot giant stars, the companion may be much brighter than the accretion disk in the optical band. The orbital inclination of ANSB systems may also partly contribute to the magnitude difference between the disk and the companion, i.e., the larger the inclination angle, the less flux from the accretion disk, and the more the system looks like normal stars.

The types of falsely classified normal stars are also important for analyzing the performance of the classification model. In Figure 6, we show the falsely classified normal stars in the CMD. For the single stars, most false classifications are the MS stars, which with mass range $0.8 \sim 2.0\,M_{\odot}$ and $7.4 \sim 9.9\,M_{\odot}$. For the binary stars, most false classifications are MS+MS with both mass $\lesssim 2.0\,M_{\odot}$, MS+MS with one or both mass $\gtrsim 6.0\,M_{\odot}$, WD or double WD binaries.

In Figure 7, we show the falsely classified ANSB systems and normal stars in the color–color diagram (CCD). The lower left part of Figure 7 corresponds to those ANSB systems whose accretion disks are brighter than their companions and some massive MS single or binary stars. The upper right part of Figure 7 corresponds to those ANSB systems whose accretion disks are dimmer than their companions, and some low-mass MS single or binary stars, WD, or double WD binaries. It is clearly shown in Figure 7 that falsely classified ANSB and normal stars highly overlap with each other.

Actually, the false classifications are derived from the fact that there are great resemblances between some ANSBs and normal binaries under the CSST photometric system. Figure 8 shows two examples where ANSBs are quite similar to normal binaries, and even machine learning cannot classify them correctly only by the seven CSST magnitudes. Maybe, a slitless spectrum from the CSST survey might help to solve this problem.

3.2. IAD

Similar to the left panel of Figure 1, but with X-ray reprocessing effect, Figure 9 shows the evolution tracks of two typical ANSBs in CMD. For a specific system, the flux of IAD is higher than that of classical MCD. In other words, the accretion disk becomes the dominant part of the flux from most ANSBs. Evolution tracks in Figure 9 exhibit relatively bluer color and higher brightness in CMD compared to Figure 1. Due to the constraints of the Eddington limit, a part of the tracks in Figure 9 appear as straight lines.

Figures 10 and 11 show the SED of the beginning and end of the mass transfer for two systems as shown in Figures 2 and 3. Compared with the left panels of Figures 2, 3 and 10, 11, when the mass transfer rate is high, the flux of the accretion disk at the optical band is significantly enhanced due to the X-ray reprocessing effect. Compared with the right panels of Figures 2, 3 and 10, 11, when the mass transfer rate is low, the appearance of ANSB at the optical band is not significantly affected by the X-ray reprocessing effect. We notice that more ANSB systems become accretion disk-dominated systems after considering the X-ray reprocessing effect. The accretion disk may be dimmer than the companion star only when the mass transfer rate of the system is low enough and/or the companion star evolves into a brighter giant star or the orbital inclination angle is large.

Table 3 shows the classification results of the test set with the X-ray reprocessing effect. Classification accuracy of ANSBs is 96.83%, and can still exceed 99% for normal stars. So, no matter whether we consider the X-ray reprocessing effect cannot significantly affect the classification accuracy of ANSBs we considered here, based on the CSST photometric

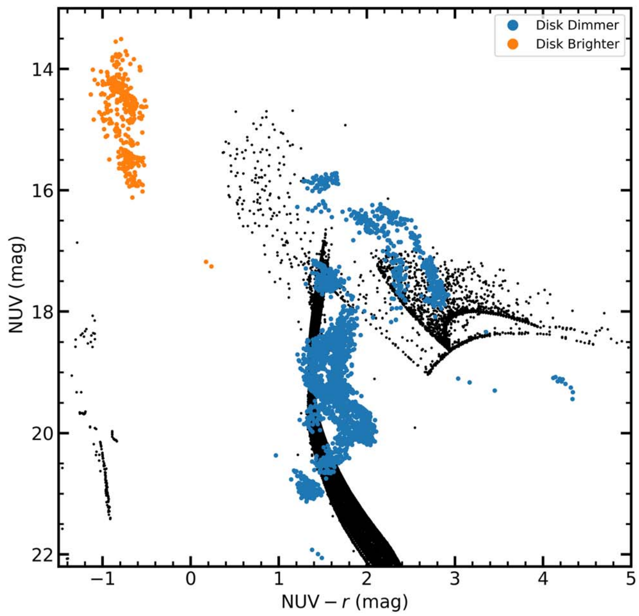

Figure 4. (Left) Distribution of the falsely classified ANSB systems in which the accretion disk is brighter or dimmer than the companion star in CMD. (Right) The distribution of the falsely classified ANSBs for systems with different orbital inclination angles in CMD. Black dots represent background normal stars, where only the sample of 1 Gyr is shown as a position reference for simplicity. The distance is set to 10 kpc.

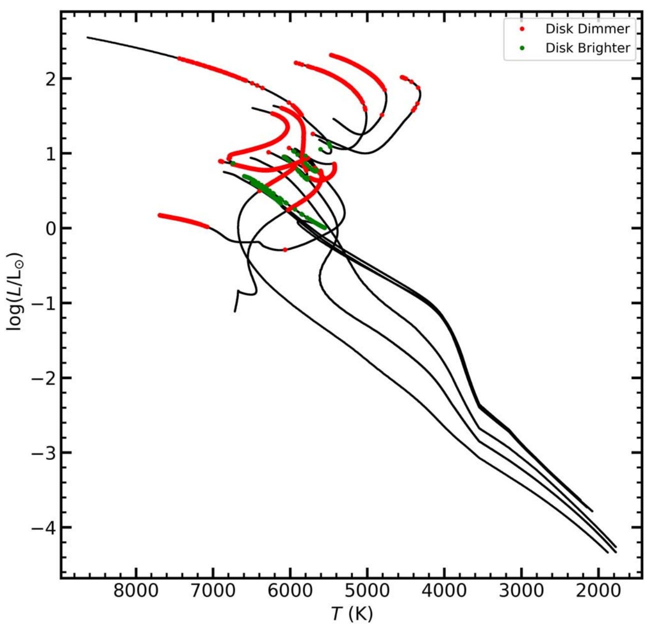

Figure 5. Evolutionary tracks of the companions of all ANSB systems in our models. Colored dots represent the companions in the falsely classified ANSB systems.

system. This is because the flux of our ANSB is roughly the superposition of an accretion disk spectrum and a blackbody spectrum, while the flux of a normal single (binary) star is roughly a blackbody spectrum (the superposition of two blackbody spectra). Therefore, no matter whether we consider this effect, most of our ANSBs are quite different from normal stars.

Figures 12–14 show the falsely classified ANSBs and normal stars. The distribution of falsely classified ANSBs is similar to the results in Section 3.1. When the companion star is a giant star and/or the mass transfer rate is low, or the orbital inclination angle is large, the accretion disk may be dimmer than the companion star at the optical band. Among these falsely classified ANSBs, ANSBs with large orbital inclination angles are still dominant, because their SEDs are very similar to blackbody spectra at the optical band. The falsely classified normal background stars can be divided into three groups: MS stars with a mass range of $0.9 \sim 2.65\,M_{\odot}$, MS stars with a mass $\gtrsim 6.50\ M_{\odot}$, and single/double WDs. Among the three groups, the first two groups are dominant. The relative number of falsely classified WD systems is larger compared with Section 3.1. This situation is from the fact that the SED of some ANSBs is closer to WD or double WD binary at the optical band after considering the X-ray reprocessing effect.

In Figure 15, we show the falsely classified ANSB systems and normal stars in CCD. Similar to Figure 8, the falsely classified ANSB systems and normal stars highly overlap with each other. Figure 16 shows examples where ANSBs are quite

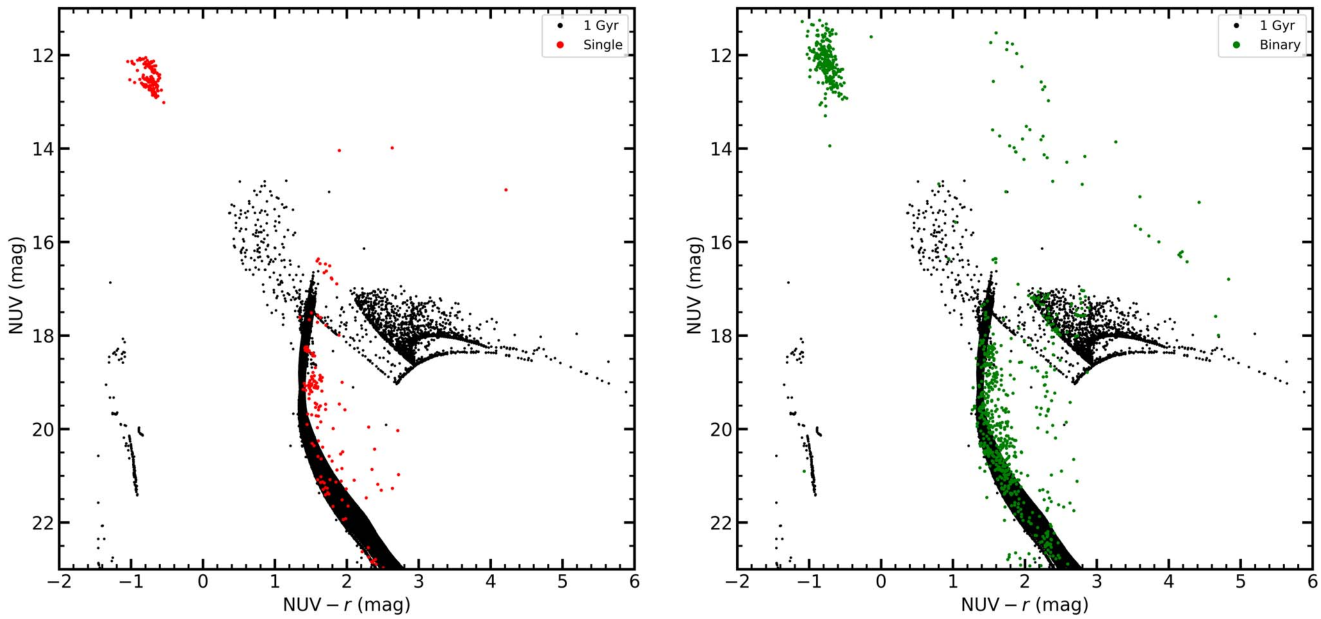

Figure 6. Left and right show falsely classified normal single and binary stars respectively. The distance is set to 10 kpc.

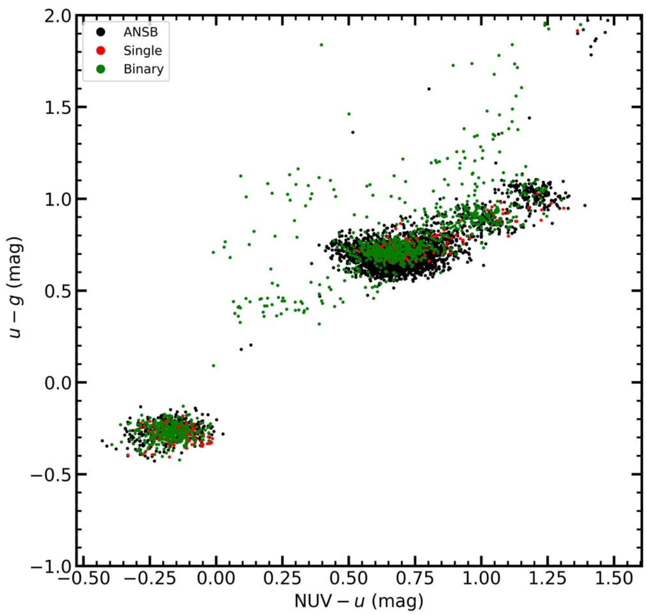

Figure 7. False classification results in CCD. Black dots represent falsely classified ANSBs. The red and green dots represent falsely classified single and binary stars, respectively.

similar to normal binaries. Machine learning may not be able to distinguish between such ANSBs and normal binaries only by seven CSST photometric magnitudes.

As a conclusion, whether or not we consider the X-ray reprocessing effect has little influence on the machine learning classification efficiency of ANSBs.

4. Discussion

In this paper, we investigate whether or not machine learning can efficiently search for ANSB potential candidates from the CSST photometric system. We consider two different accretion disk radiation mechanisms, i.e., the classical MCD model and the IAD model, and compare their impact on machine learning classification efficiency. We find that the classification accuracies are 97.05% and 96.83% for the MCD and the IAD models respectively.

From the results, the X-ray reprocessing effect does not have a significant impact on the classification results. This situation is due to the fact that the flux of a normal binary star is roughly taken as the superposition of two blackbody spectra. However, the flux of our ANSB is the superposition of the accretion disk spectrum and blackbody spectrum. Whether or not we consider the IAD model, most of our ANSBs are quite different from normal binaries. However, to find ANSB candidates, a classification model that considers the X-ray reprocessing effect into account is more meaningful.

In this paper, we choose the AIC channel to produce NS. The surface chemical abundance of companions of ANSBs that are produced by the AIC channel may be different from that from the standard channel, which may change the instability of the accretion disks and thus affect the timescales which the ANSBs are in the quiescent state (e.g., Lasota et al. 2008; Tauris et al. 2013). Although the initial parameter spaces to form an ANSB may be different for different evolutionary channels, it is difficult to distinguish which channel the ANSB is from by observations (Tauris et al. 2013). As a result, the

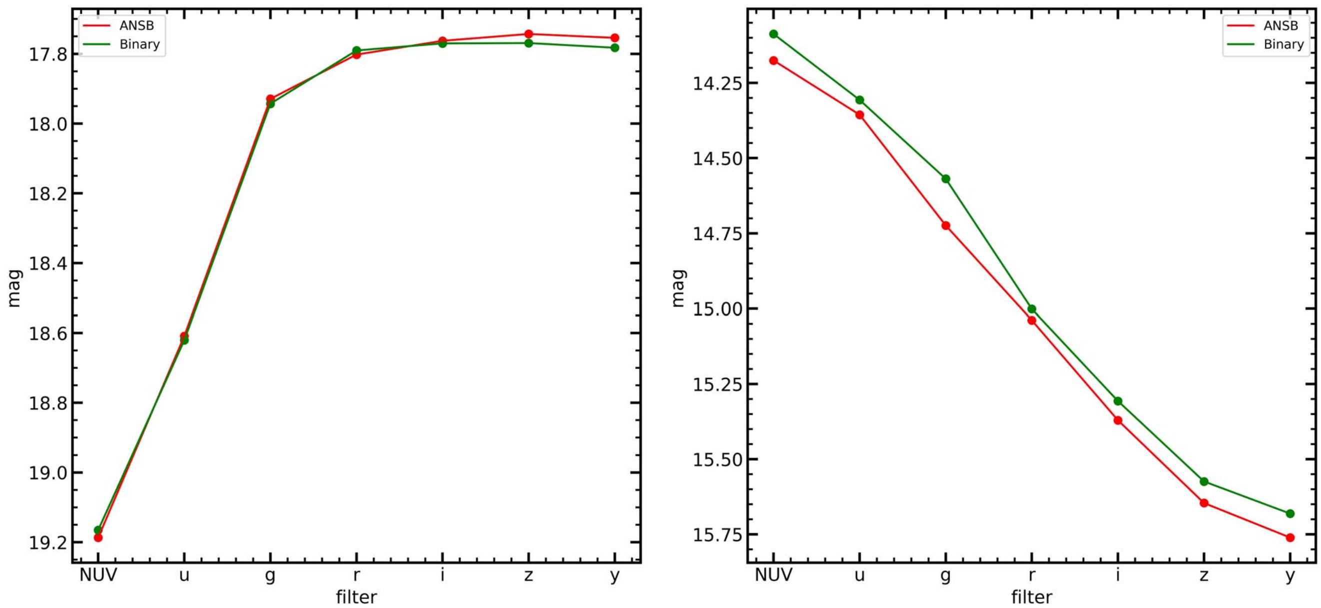

Figure 8. Two examples of ANSBs which are similar to normal binaries under the CSST photometric system. (Left) The red line is an ANSB with ($M_{\rm NS}$, M_2) = (1.3479 $M_\odot$, 0.6398 $M_\odot$), while the green is a binary system consisting of a CO WD + MS with ($M_{\rm COWD}$, $M_{\rm MS}$) = (0.6529 $M_\odot$, 1.5186 $M_\odot$). (Right) The red line is an ANSB with ($M_{\rm NS}$, M_2) = (1.2505 $M_\odot$, 2.5292 $M_\odot$), while the green line is a binary system consisting of a MS + MS with ($M_{\rm MS,1}$, $M_{\rm MS,2}$) = (6.5055 $M_\odot$, 0.7189 $M_\odot$). The distance is set to 10 kpc.

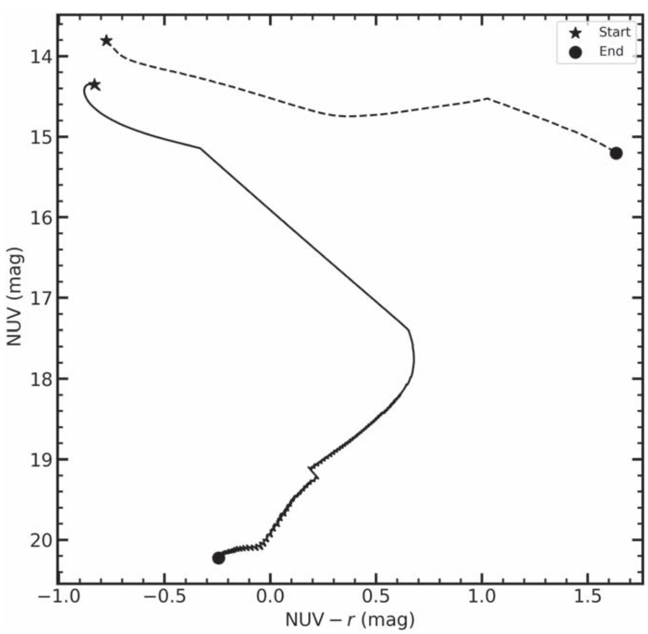

Figure 9. Similar to the left panel of Figure 1, but with X-ray reprocessing effect.

different evolutionary channels will not affect our basic conclusion.

In addition, in this paper, the ANSBs are produced based on some simple assumptions, i.e., the radiation comes from the accretion disk and the companion only. For example, the corona of the NS was neglected (e.g., Markoff et al. 2005); heating of the companion star is also ignored (e.g., Harlaftis et al. 1997; Romani & Sanchez 2016). These effects that we neglected could become important in some special ANSBs. We also do not consider the effect of emission lines, which could affect the accuracy of the classification model. In the future, we will add these effects step by step to improve our classification model. A full and accurate ANSB model will make our results more robust, although the simplified model here already yields meaningful insights.

Furthermore, we assume that the NS is a point mass. When a Schwarzschild black hole with the same mass of an NS in our ANSB accreting material from its companion, the inner radius of the accretion disk is about $3R_s \sim 10$–12 km (R_s is the Schwarzschild radius) (Frank et al. 2002), as a result, our classification model could not be able to distinguish between some accreting black hole binaries and part of our ANSBs.

Finally, the accreting WD binaries (AWDBs) could affect the accuracy of classification models. We make use of the AWDBs produced by Xie & Chen (2022) to test the influence of the AWDBs. We first do not consider the X-ray reprocessing effect and use our classification model to make classification predictions on these AWDBs: 2.30% of AWDBs are falsely classified as ANSBs. We then use our classification model trained in Section 2.2 to make classification predictions on these AWDBs: 8.36% of AWDBs are falsely classified as ANSBs. The above tests show that AWDBs may not

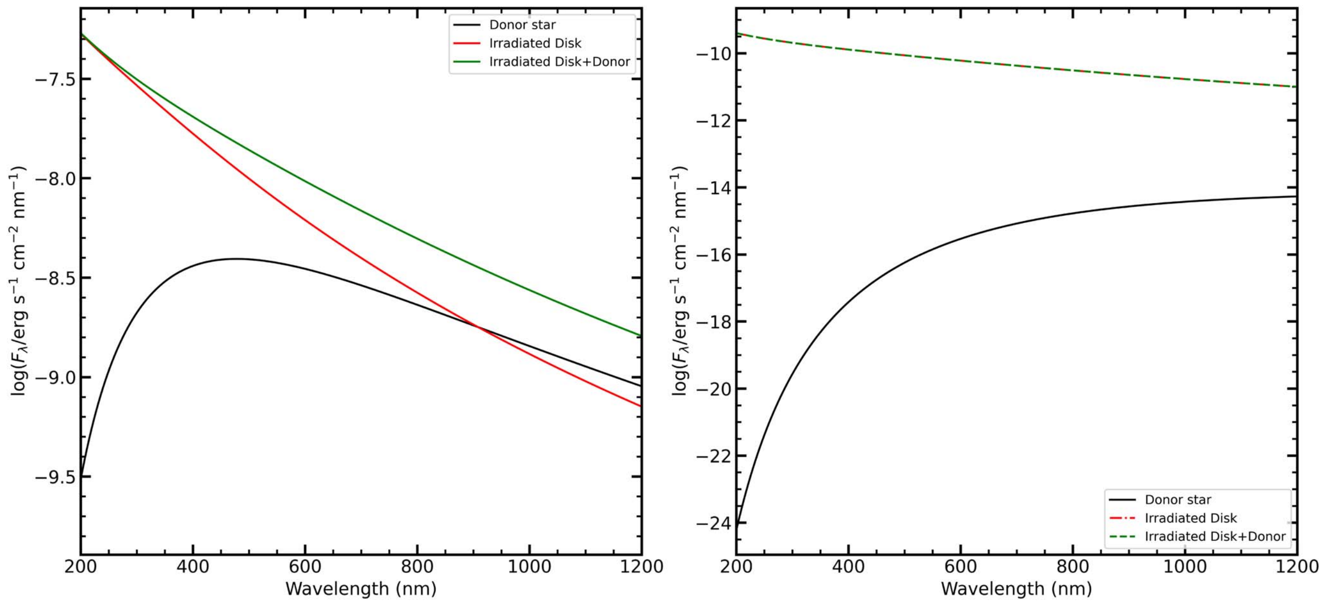

Figure 10. Similar to Figure 2, but with X-ray reprocessing effect.

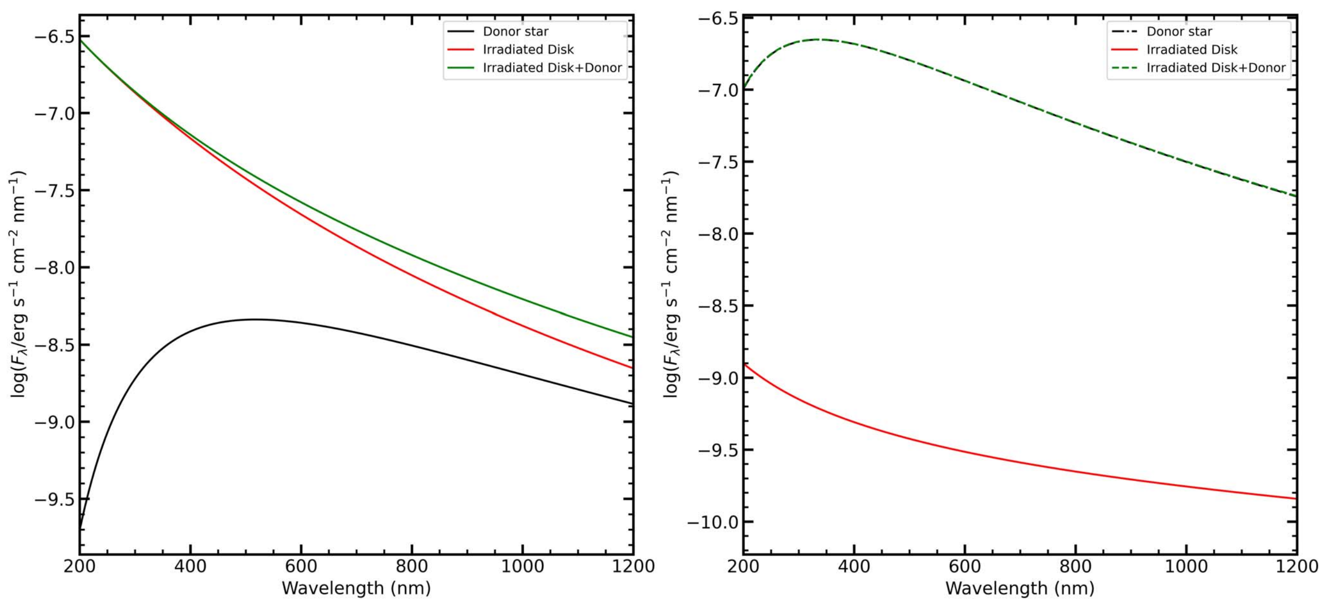

Figure 11. Similar to Figure 3, but for the system with X-ray reprocessing effect.

Table 3
Classification Results of the Test Set with X-Ray Reprocessing Effect

	All	Falsely Classified	Correctly Classified
ANSBs	118,225	2770	115,455
Normal Stars	1,452,573	3779	1,448,794
All	1,570,798	6549	1,564,249

significantly affect our classification model. We think this situation may be due to the fact that the flux of an AWDB in Xie & Chen (2022) is still roughly the superposition of two blackbody spectra: the accreting white dwarf and the companion star, which are quite different from those of ANSBs.

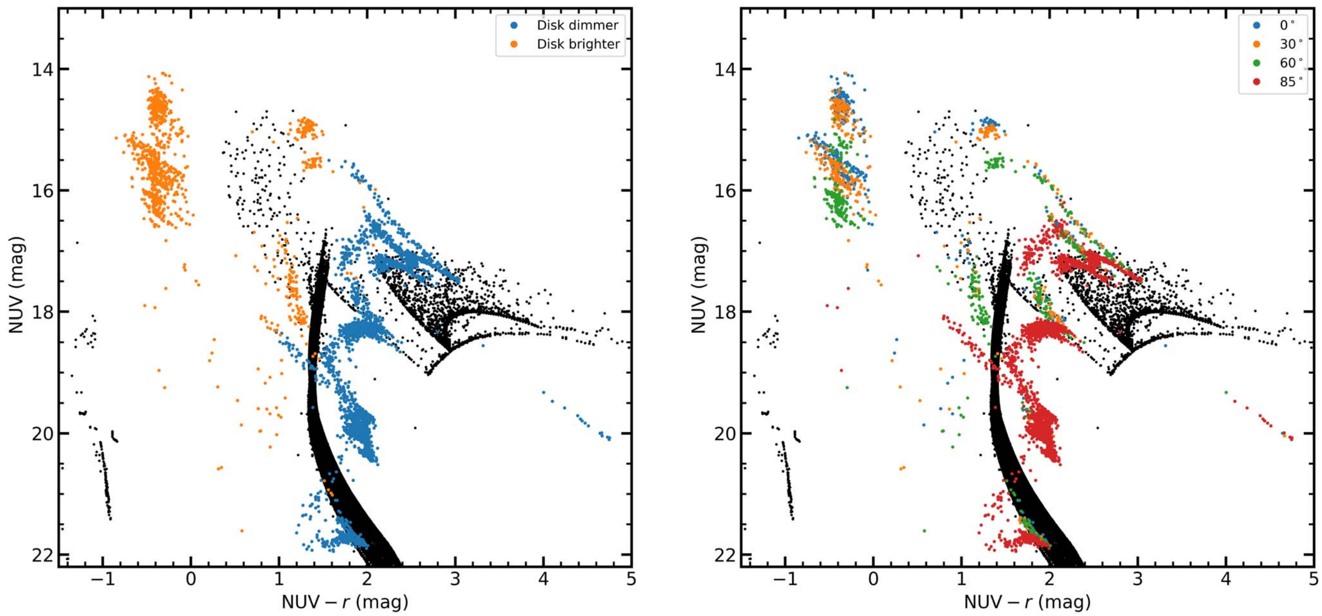

Figure 12. Similar to Figure 4, but with the X-ray reprocessing effect.

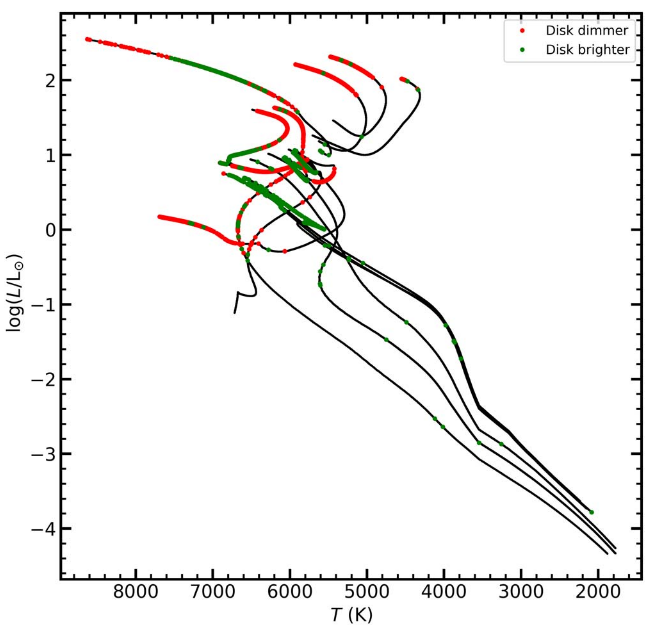

Figure 13. Similar to Figure 5, but with the X-ray reprocessing effect.

5. Conclusions

In this paper, we produced some ANSBs and normal binary stars to investigate if machine learning can efficiently search for the ANSB candidates under the CSST photometric system. Our classification results indicate that machine learning can efficiently select out the ANSB candidates from the background normal stars. The classification accuracy of ANSBs in our simulated data set can exceed 96%, with or without the X-ray reprocessing effects.

For the falsely classified systems, we find that if the magnitude difference between the accretion disk and the companion of an ANSB is too large, machine learning has a higher probability of misclassifying it as a normal star. When the accretion disk is much brighter than the companion, machine learning may misclassify such an ANSB as a massive single or binary MS star. When the companion is much brighter than the accretion disk, i.e., when the mass transfer rate of the system is low and/or the companion star evolves to a bright giant star, or the orbital inclination angle is too large, the machine learning may misclassify such an ANSB as a less massive MS, and WD

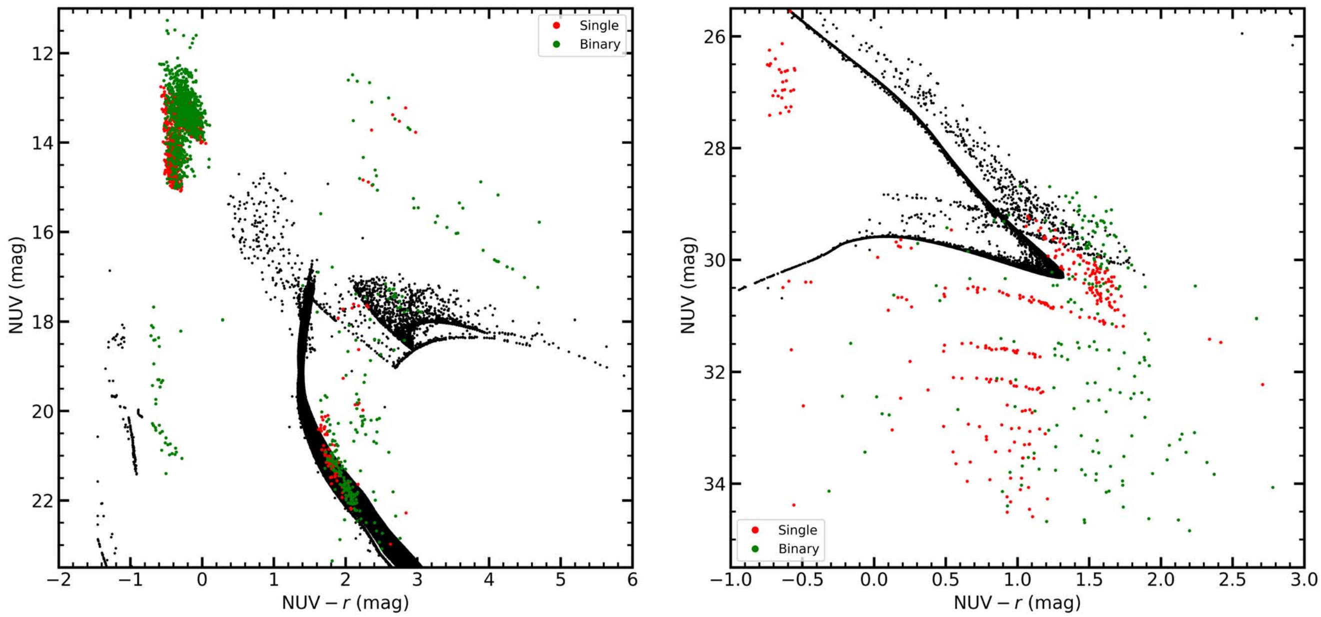

Figure 14. Falsely classified normal background single and binary stars. (Left) Objects near the MS belt. (Right) Objects near the WD branch. The distance is set to 10 kpc.

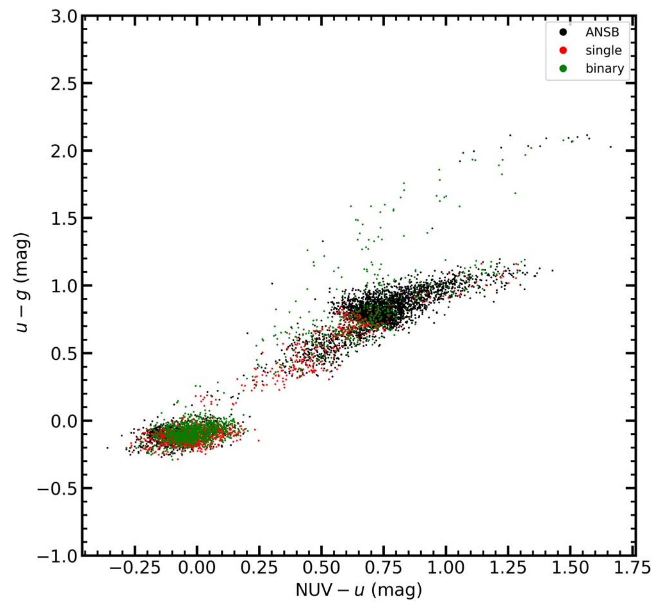

Figure 15. Similar to Figure 7, but with the X-ray reprocessing effect.

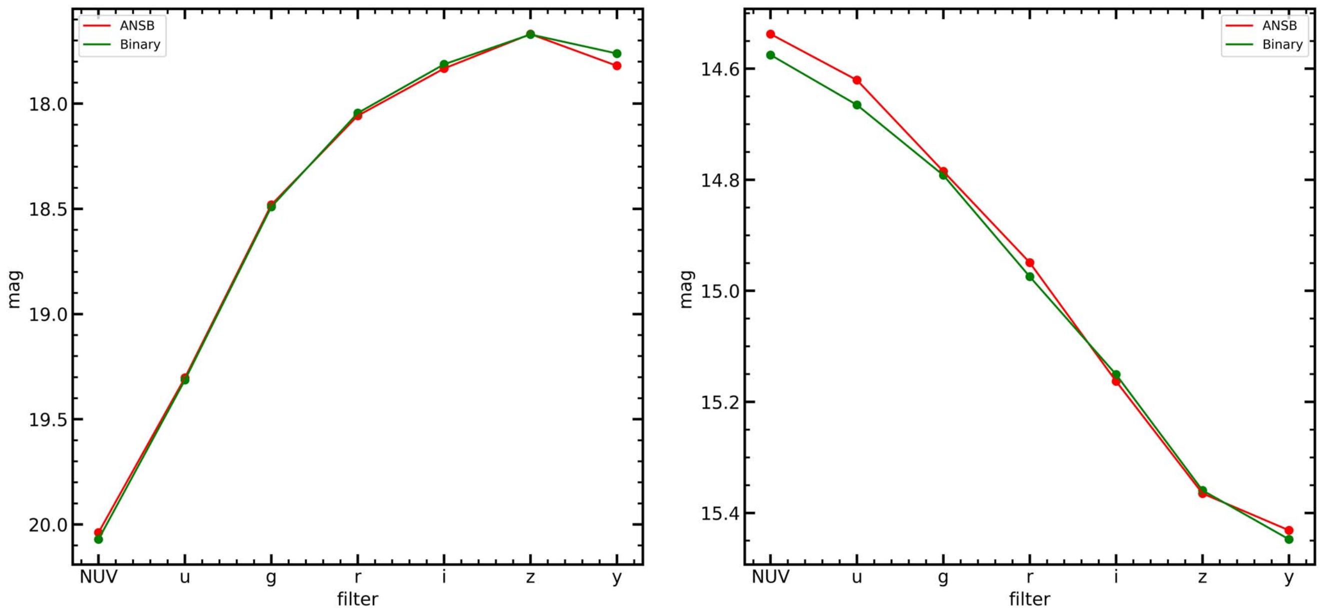

Figure 16. Similar to Figure 8, but with X-ray reprocessing effect. (Left) The red line is an ANSB with ($M_{\rm NS}$, M_2) = (1.3235 $M_\odot$, 0.7224 $M_\odot$), while the green is a binary system consisting of an MS + MS with ($M_{\rm MS,1}$, $M_{\rm MS,2}$) = (1.3022 $M_\odot$, 1.2887 $M_\odot$). (Right) The red line is an ANSB with ($M_{\rm NS}$, M_2) = (1.2513 $M_\odot$, 2.1225 $M_\odot$), while the green line is a binary system consisting of an MS + MS with ($M_{\rm MS,1}$, $M_{\rm MS,2}$) = (6.7624 $M_\odot$, 0.9538 $M_\odot$). The distance is set to 10 kpc.

binary. Maybe the slitless spectrum from the CSST survey might be helpful to increase classification accuracy further.

Acknowledgments

This work was supported by the National Key R&D Program of China with No. 2021YFA1600403 and the National Natural Science Foundation of China under grant Nos. 11973080 and 11733008. We acknowledge the science research grants from the China Manned Space Project with No. CMS-CSST-2021-B07. X.M. acknowledges the support by the Yunnan Ten Thousand Talents Plan—Young & Elite Talents Project, and CAS "Light of West China" Program.

ORCID iDs

Kai-Fan Ji https://orcid.org/0000-0001-8950-3875

References

Ambrosino, F., Miraval Zanon, A., Papitto, A., et al. 2021, NatAs, 5, 552
Archibald, A. M., Stairs, I. H., Ransom, S. M., et al. 2009, Sci, 324, 1411
Baillot d'Etivaux, N., Guillot, S., Margueron, J., et al. 2019, ApJ, 887, 48
Bassa, C. G., Patruno, A., Hessels, J. W. T., et al. 2014, MNRAS, 441, 1825
Bhattacharya, D., & van den Heuvel, E. P. J. 1991, PhR, 203, 1
Cao, Y., Gong, Y., Meng, X.-M., et al. 2018, MNRAS, 480, 2178
Chen, Y., Girardi, L., Fu, X., et al. 2019, A&A, 632, A105
Coriat, M., Fender, R. P., & Dubus, G. 2012, MNRAS, 424, 1991
Cumming, A. 2004, NuPhS, 132, 435
de Jong, J. A., van Paradijs, J., & Augusteijn, T. 1996, A&A, 314, 484
di Salvo, T., Burderi, L., Riggio, A., Papitto, A., & Menna, M. T. 2008, MNRAS, 389, 1851
Frank, J., King, A., & Raine, D. J. 2002, Accretion Power in Astrophysics (3rd ed.; Cambridge: Cambridge Univ. Press)
Ghosh, P., & Lamb, F. K. 1979, ApJ, 232, 259
Gong, Y., Liu, X., Cao, Y., et al. 2019, ApJ, 883, 203
Harlaftis, E. T., Charles, P. A., & Horne, K. 1997, MNRAS, 285, 673
Hartman, J. M., Patruno, A., Chakrabarty, D., et al. 2008, ApJ, 675, 1468
Homan, J., Buxton, M., Markoff, S., et al. 2005, ApJ, 624, 295
Hurley, J. R., Pols, O. R., & Tout, C. A. 2000, MNRAS, 315, 543
Hurley, J. R., Tout, C. A., & Pols, O. R. 2002, MNRAS, 329, 897
Jaodand, A. D., Hernández Santisteban, J. V., Archibald, A. M., et al. 2021, arXiv:2102.13145
Kubota, A., Tanaka, Y., Makishima, K., et al. 1998, PASJ, 50, 667
Lasota, J.-P. 2001, NewAR, 45, 449
Lasota, J. P., Dubus, G., & Kruk, K. 2008, A&A, 486, 523
Liu, Q. Z., van Paradijs, J., & van den Heuvel, E. P. J. 2007, A&A, 469, 807
Markoff, S., Nowak, M. A., & Wilms, J. 2005, ApJ, 635, 1203
Meng, X., Chen, X., & Han, Z. 2009, MNRAS, 395, 2103
Meng, X., & Podsiadlowski, P. 2017, MNRAS, 469, 4763
Mitsuda, K., Inoue, H., Koyama, K., et al. 1984, PASJ, 36, 741
Papitto, A., Ferrigno, C., Bozzo, E., et al. 2013, Natur, 501, 517
Patruno, A., & Watts, A. L. 2021, in Astrophysics and Space Science Library, Vol. 461, ed. T. M. Belloni, M. Méndez, & C. Zhang, 143
Patruno, A., Wette, K., & Messenger, C. 2018, ApJ, 859, 112
Patterson, J. 1984, ApJS, 54, 443
Pedregosa, F., Varoquaux, G., Gramfort, A., et al. 2011, JMLR, 12, 2825
Podsiadlowski, P., Rappaport, S., & Pfahl, E. D. 2002, ApJ, 565, 1107
Ritter, H., & Kolb, U. 2003, A&A, 404, 301
Romani, R. W., & Sanchez, N. 2016, ApJ, 828, 7
Russell, D. M., Fender, R. P., Hynes, R. I., et al. 2006, MNRAS, 371, 1334
Tauris, T. M., Sanyal, D., Yoon, S. C., & Langer, N. 2013, A&A, 558, A39
Tutukov, A. V., Fedorova, A. V., Ergma, E. V., & Yungelson, L. R. 1985, SvAL, 11, 52
van der Sluys, M. V., Verbunt, F., & Pols, O. R. 2005a, A&A, 431, 647
van der Sluys, M. V., Verbunt, F., & Pols, O. R. 2005b, A&A, 440, 973
van Paradijs, J., & McClintock, J. E. 1994, A&A, 290, 133
Vaughan, B. A., van der Klis, M., Wood, K. S., et al. 1994, ApJ, 435, 362
Vrtilek, S. D., Raymond, J. C., Garcia, M. R., et al. 1990, A&A, 235, 162
Wang, B. 2018, MNRAS, 481, 439
Wang, B., Liu, D., & Chen, H. 2022, MNRAS, 510, 6011
Wang, S., & Chen, X. 2019, ApJ, 877, 116
Wijnands, R., & van der Klis, M. 1998, Natur, 394, 344
Xie, W., & Chen, H.-L. 2022, RAA, 22, 055003
Xin, Y., Ferraro, F. R., Lu, P., et al. 2015, ApJ, 801, 67